

Elastohydrodynamic instabilities of a soft robotic arm in a viscous fluid

Mohamed Warda*

*Cavendish Laboratory, University of Cambridge, J.J. Thomson Avenue, Cambridge CB3 0US, United Kingdom and
Department of Applied Mathematics and Theoretical Physics, Centre for Mathematical Sciences,
University of Cambridge, Cambridge CB3 0WA, United Kingdom*

Ronojoy Adhikari

*Department of Applied Mathematics and Theoretical Physics, Centre for Mathematical Sciences,
University of Cambridge, Cambridge CB3 0WA, United Kingdom*

The design and control of soft robots operating in fluid environments requires a careful understanding of the interplay between large elastic body deformations and hydrodynamic forces. Here we show that this interplay leads to novel elastohydrodynamic instabilities in a clamped soft robotic arm driven terminally by a constant pressure in a viscous fluid. We model the arm as a Cosserat rod that can stretch, shear and bend. We obtain invariant, geometrically exact, non-linear equations of motion by using Cartan's method of moving frames. Stability to small perturbations of a straight rod is governed by a non-Hermitian linear operator. Eigenanalysis shows that stability is lost through a Hopf bifurcation with the increase of pressure above a first threshold. A surprising return to stability is obtained with further increase of pressure beyond a second threshold. Numerical solutions of the non-linear equations, using a geometrically exact spectral method, confirms stable limit-cycle oscillations between these two pressure thresholds. An asymptotic analysis in the beam limit rationalizes these results analytically. This counterintuitive sequence of bifurcations underscores the subtle nature of the elastohydrodynamic coupling in Cosserat rods and emphasizes their importance for the control of the viscous dynamics of soft robots.

I. INTRODUCTION

The geometric dynamics of articulated arms has been studied extensively due to their importance in robotics [1–3]. In the emerging field of soft robotics, arms with continuously distributed articulations have been constructed and studied with applications, among others, to minimally invasive surgery [4, 5] and medical robotics [6, 7]. Since each cross-section of such a continuous soft robotic arm has the full degrees of freedom of a rigid body, the deformation of the arm must include stretch, shear, bend and twist. The classical beam theories do not include all of these degrees of freedom [8–10] and more complete descriptions of a soft slender body then become necessary. The special theory of Cosserat rods provides such a description and has been used to model soft robotic arms [6, 7, 11–15].

When soft robotic arms operate in a fluid environment, the fluid-structure interaction must be included in the balance of forces and torques. Recent work has investigated this fluid-structure interaction [15] at finite Reynolds numbers. On the other hand, in many biological settings the fluid-structure interaction is governed by slow viscous flow. In fact, this approximation has been widely used to study the dynamics of filaments in viscous fluids. Elastohydrodynamic instabilities of terminally driven filaments have recently been studied in this approximation [16–23]. These studies have revealed oscillatory flutter instabilities that arise through Hopf bifurcations. They are related to non-conservative problems

in structural stability, for instance Beck's column [24–30]. The Euler-Bernoulli model in [17] has been further developed and studied in subsequent work [18–21, 23], exploring both the linear instability mechanisms and the rich nonlinear dynamics of filaments driven by follower forces. The effect of fluid viscoelasticity elastohydrodynamic instabilities has been studied recently [22].

While there is a vast literature on such elastohydrodynamic instabilities of filaments in viscous fluids, the majority of existing work models filaments as inextensible and unshearable slender structures. In contrast, we study the dynamics of a soft robotic arm including the fluid-structure interaction in the limit of slow viscous flow. This yields elastohydrodynamic equations where the additional degrees of freedom provided by the Cosserat theory are included. The forces and torques acting on the rod due to motion in the ambient fluid are included, in the Stokes approximation, as proportional to the local velocity and angular velocity of the rod. Working in the overdamped limit, we derive the geometrized equations of motion for the Cosserat rod in a coordinate-invariant and geometrically exact manner in terms of a geometric field theory [31].

Using these equations of motion, we study the response of the soft robotic arm to an externally applied terminal pressure, as might be obtained when the arm makes contact with an underwater obstacle. The linearization of the field theory reveals a subtle interplay between the Cosserat degrees of freedom and leads to non-hermitian equations of motion. While the “filament limit” or “beam limit” of our field theory show excellent agreement with the results found in [17, 21, 23], deviations from these limits reveal both qualitatively and quantitatively differ-

* mrmaw2@cam.ac.uk

ent features of the dynamics. We find that incorporating shear and angular dissipation into the model leads to a monotonic reduction of the critical values of the follower force. Allowing for Cosserat degrees of freedom, we find a loss of stability through a Hopf bifurcation for values of pressure that are smaller compared to the case of inextensible and unshearable filaments. More crucially, we find that the stretch degree of freedom in rods that can sustain large compression results in non-trivial alterations to the stability. In particular, we identify regimes in parameter space where the rod loses stability through a Hopf bifurcation and subsequently regains stability for larger values of the pressure. Additionally, we identify regimes where the stretching eliminates the Hopf bifurcation entirely and no loss of stability is observed. To complement our linear stability analysis, we numerically integrate the geometric field theory by means of a geometrically exact numerical scheme that reveals stable limit cycle oscillations. This corresponds to the sustained beating of the rod under applied pressure.

The rest of the paper is outlined as follows. In Section II, we summarize the geometric field theory formalism that we employ in this work, which is presented in detail in [31]. In Section III, we present our constitutive model for the viscous elastohydrodynamics of a soft robotic arm and derive covariant equations of motion as systems of nonlinear PDEs. In Section IV we impose boundary conditions corresponding to a pressure applied to one terminus of the rod to model a pressure-driven robotic arm, highlighting its role in injecting and dissipating energy into the system. We linearize the field theory in Section V, identifying the circulatory nature of the pressure-driven model in the process and write down the equations of motion in terms of a non-Hermitian linear operator. We then present the results of our linear stability analysis in Section VI and the results of our nonlinear numerical simulations in Section VII. In Section VIII, we connect our work to the existing literature on filaments by deriving a “partial beam limit” that elucidates the counterintuitive spectrum observed in Section VI. We conclude by summarizing and discussing extensions of our study.

II. GEOMETRIC FIELD THEORY FOR PLANAR COSSERAT RODS

The configuration of a Cosserat rod at time t is described by its centerline $\mathbf{r}(u, t)$ and three orthonormal frame vectors $\mathbf{e}_1(u, t), \mathbf{e}_2(u, t), \mathbf{e}_3(u, t)$, rigidly attached to the cross-section at material parameter u . We choose \mathbf{e}_1 to be normal to the cross-section and \mathbf{e}_2 and \mathbf{e}_3 to span the plane of the cross-section. We restrict ourselves in this work to configurations in which the centerline remains in the plane and the \mathbf{e}_3 is normal to the plane. Then, the configuration of the rod is given by a 3×3

matrix-valued field

$$\varphi(u, t) = \begin{bmatrix} 1 & 0 & 0 \\ \mathbf{r}(u, t) & \mathbf{e}_1(u, t) & \mathbf{e}_2(u, t) \end{bmatrix}, \quad (1)$$

where each column vector has two components relative to a fixed frame. The matrix is a representation of $SE(2)$, the Lie group of proper rigid motions in the Euclidean plane. The spatial and temporal derivatives of the configuration, when resolved in the moving frame provided by \mathbf{e}_1 and \mathbf{e}_2 , can be expressed as

$$\partial_t \varphi = \varphi V, \quad \partial_u \varphi = \varphi E, \quad (2)$$

where V and E are matrices in the Lie algebra $\mathfrak{se}(2)$. This Lie algebra is three-dimensional and its elements can be expressed in the canonical basis. The components of the velocity V and deformation E in this canonical basis are $V_\alpha = (v_1, v_2, \Omega)$ and $E_\alpha = (h_1, h_2, \Pi)$. In terms of the centerline and frame vectors we have

$$\begin{aligned} v_1 &= \mathbf{e}_1 \cdot \partial_t \mathbf{r}, & v_2 &= \mathbf{e}_2 \cdot \partial_t \mathbf{r}, & \Omega &= \mathbf{e}_2 \cdot \partial_t \mathbf{e}_1, \\ h_1 &= \mathbf{e}_1 \cdot \partial_u \mathbf{r}, & h_2 &= \mathbf{e}_2 \cdot \partial_u \mathbf{r}, & \Pi &= \mathbf{e}_2 \cdot \partial_u \mathbf{e}_1. \end{aligned} \quad (3)$$

These components, and therefore the matrices V and E , are invariant under rigid motions $\mathbf{r} \rightarrow \mathbf{R} \cdot \mathbf{r} + \mathbf{b}$ and $\mathbf{e}_i \rightarrow \mathbf{R} \cdot \mathbf{e}_i$ where \mathbf{R} is a proper orthogonal matrix and \mathbf{b} is an arbitrary vector in the plane. The element of arc of the centerline is $ds = \sqrt{h_1^2 + h_2^2} du$, h_1 and h_2 are measures of shear of the cross-section and Π is a measure of the bending of the centerline. At any instant, the configuration of the rod can be recovered up to a rigid motion given E . Conversely, two configurations with identical values of E can only differ by a rigid motion.

The equality of mixed partial derivatives of the configuration, $\partial_u \partial_t \varphi = \partial_t \partial_u \varphi$, immediately yields the compatibility condition

$$\partial_t E = \partial_u V + [E, V] \equiv \mathcal{D}V. \quad (4)$$

Here $\mathcal{D} = \partial_u + \text{ad}_E$ is a covariant derivative that acts on elements of the Lie algebra. We list the appropriate covariant derivatives, adjoint maps, and their duals, in the Appendix A.

In the absence of inertia, we may write down the dynamics of the Cosserat rod covariantly in terms of a generalized stress Σ and generalized body force density j in the dual Lie algebra $\mathfrak{se}(2)^*$. The components in the canonical dual basis are $\Sigma_\alpha = (F_1, F_2, M)$ and $j_\alpha = (f_1, f_2, m)$. The generalized balance law in terms of these components is

$$\mathcal{D}_{\alpha\beta}^* \Sigma_\beta + j_\alpha = 0, \quad (5)$$

where $\mathcal{D}^* = \partial_u + \text{ad}_E^*$ is a dual covariant derivative that acts on elements of the dual Lie algebra.

The principle of material indifference requires constitutive laws to be invariant under rigid motions. This invariance is most easily imposed by expressing the kinematic and dynamic equations in the moving frame. Then,

kinematic quantities take values in the Lie algebra $\mathfrak{se}(2)$ and dynamic quantities take values in the dual Lie algebra $\mathfrak{se}(2)^*$. In this paper, we restrict ourselves to rheological constitutive laws of the form $\Sigma_\alpha = \Sigma_\alpha(E_\alpha)$ and dynamical constitutive laws of the form $j_\alpha = j_\alpha(V_\alpha)$.

We note that Eq. (5) is covariant in the following sense. For a constant $SE(2)$ group element g , the rigid transformation $\varphi \rightarrow g\varphi$ leaves V and E invariant, which is easily deduced from their definitions. It is then evident that specifying constitutive laws $\Sigma_\alpha = \Sigma_\alpha(E_\alpha)$ and $j_\alpha = j_\alpha(V_\alpha)$ leads to the invariance of Eq. (5) under rigid motions.

III. VISCOUS ELASTOHYDRODYNAMICS

We now make constitutive choices that are appropriate for a soft robotic arm in a viscous fluid. We consider a Cosserat rod of rest length L and a stress-free configuration

$$\bar{r}(u) = (u, 0), \quad \bar{e}_1(u) = (1, 0), \quad \bar{e}_2(u) = (0, 1). \quad (6)$$

The components of the deformation in this configuration are $\bar{E}_\alpha = (1, 0, 0)$. The strain of an arbitrary configuration with respect to this reference configuration is $E - \bar{E}$ and this is invariant under rigid motions. The linear constitutive equations for a linearly elastic Cosserat rod subject to linear Stokes drag are

$$\Sigma_\alpha = K_{\alpha\beta}(E_\beta - \bar{E}_\beta), \quad j_\alpha = -\Gamma_{\alpha\beta}V_\beta, \quad (7)$$

where $K_{\alpha\beta}$ and $\Gamma_{\alpha\beta}$ are symmetric positive definite stiffness and friction tensors respectively. For simplicity, we choose these to be diagonal, given in components by $K_{\alpha\beta} = \text{diag}(k_1, k_2, k_3)$ and $\Gamma_{\alpha\beta} = (\gamma_1, \gamma_2, \gamma_3)$. The rheological constitutive law admits an energy function

$$\begin{aligned} \mathcal{U}[\varphi] &= \frac{1}{2} \int_0^L du \langle K(E - \bar{E}), E - \bar{E} \rangle \\ &= \frac{1}{2} \int_0^L du k_1(h_1 - 1)^2 + k_2h_2^2 + k_3\Pi^2, \end{aligned} \quad (8)$$

where $\langle \cdot, \cdot \rangle$ denotes the canonical pairing between $\mathfrak{se}(2)$ and its dual. This encodes the energetic penalty for a deformation from a reference state that is a planar rod with no stretch and no shear ($h_1 = 1$, $h_2 = 0$), and no bending ($\Pi = 0$).

Substituting the constitutive relationships in Eq. (7) into the balance law in Eq. (5) gives an instantaneous relationship between the velocities and deformations,

$$\Gamma_{\alpha\beta}V_\beta = \mathcal{D}_{\alpha\beta}^*[K_{\beta\mu}(E_\mu - \bar{E}_\mu)]. \quad (9)$$

Since the deformations specify the shape of the rod and the velocities specify its motion, this key relationship provides a rigidity-invariant map between space of shapes and the space of motions. The map contains the entire dynamic content of rod motion.

The equation of motion for the configuration can be obtained explicitly using canonical coordinates (x, y, θ) for $SE(2)$,

$$\varphi(u, t) = \begin{bmatrix} 1 & 0 & 0 \\ x(u, t) & \cos \theta(u, t) & -\sin \theta(u, t) \\ y(u, t) & \sin \theta(u, t) & \cos \theta(u, t) \end{bmatrix}. \quad (10)$$

We then have two equivalent ways of formulating the equations of the Cosserat rod.

First, we may close the equation by eliminating E completely and writing three nonlinear time-dependent partial differential equations for the coordinates of the rod by combining Eq. (2), Eq. (9), and the coordinatization in Eq. (10)

$$\begin{aligned} \partial_t \varphi &= \varphi V, \quad \partial_u \varphi = \varphi E, \\ \Gamma_{\alpha\beta}V_\beta &= \mathcal{D}_{\alpha\beta}^*[K_{\beta\mu}(E_\mu - \bar{E}_\mu)]. \end{aligned} \quad (11)$$

This system requires one initial condition and two boundary conditions for φ . We focus on clamped-forced boundary conditions in this paper, of the general form

$$\varphi(0, t) = \mathbb{I}, \quad \Sigma_\alpha(L, t) = P_\alpha(t), \quad (12)$$

where stresses are enforced at the $u = L$ boundary, or tip of the Cosserat rod. We stress that this forced boundary condition is a nonlinear boundary condition on φ upon application of Eq. (7) and Eq. (2).

Second, we may impose the relation $\partial_u \varphi = \varphi E$ only at the initial time $t = 0$ and promote the compatibility condition in Eq. (4) to a time evolution equation in the Lie algebra, which enforces $\partial_u \varphi = \varphi E$ for all time. In the manner, we obtain six time-dependent partial differential equations for the coordinates of the rod and the deformations

$$\begin{aligned} \partial_t \varphi &= \varphi V, \quad \partial_t E_\alpha = \mathcal{D}_{\alpha\beta}V_\beta, \\ \Gamma_{\alpha\beta}V_\beta &= \mathcal{D}_{\alpha\beta}^*[K_{\beta\mu}(E_\mu - \bar{E}_\mu)], \end{aligned} \quad (13)$$

where the clamped-forced boundary conditions are now imposed on E via

$$\mathcal{D}_{\alpha\beta}^*\Sigma_\beta(0, t) = 0, \quad \Sigma_\alpha(L, t) = P_\alpha(t), \quad (14)$$

and an application of the constitutive law. In particular, the previously nonlinear (in φ) boundary condition $\Sigma_\alpha(L, t) = P_\alpha(t)$ is now a linear boundary condition in E , while the previously linear (in φ) clamping boundary condition is now a nonlinear boundary condition in E , obtained through setting $V(0, t) = 0$. Applying the balance law in Eq. (9) leads to $\mathcal{D}_{\alpha\beta}^*\Sigma_\beta = 0$, a “covariant Neumann” boundary condition. We note that in this formulation, the dynamical equation is time-independent and in the dual Lie algebra, the time evolution of the deformation is in the Lie algebra and the time evolution of the configuration is in the Lie group. Thus, the dynamics is partitioned over the group, the algebra and its dual algebra. We use this formulation below for numerical simulations.

IV. PRESSURE-DRIVEN SOFT ARM

We now obtain the appropriate boundary conditions for a soft robotic arm described by the elastohydrodynamic equations derived in the previous section. We assume that a pressure acts normal to a terminal cross-section and that the resultant force \mathcal{F} points along the $-e_1$ axis. In our formulation, this implies that the boundary condition at the pressurized end is

$$\Sigma_\alpha(L, t) = (-\mathcal{F}, 0, 0). \quad (15)$$

This is the so-called follower force model, which is most conveniently expressed in the body frame of the rod. We anticipate an interesting feature of the dynamics through the following observation. Differentiating the energy with respect to time gives

$$\begin{aligned} \frac{d\mathcal{U}}{dt} &= \int_0^L du \langle K(E - \bar{E}), \partial_t E \rangle \\ &= \int_0^L du \langle \Sigma, \mathcal{D}V \rangle \\ &= \langle \Sigma(L, t), V(L, t) \rangle - \int_0^L du \langle \mathcal{D}^* \Sigma, V \rangle \quad (16) \\ &= \langle \Sigma(L, t), V(L, t) \rangle - \int_0^L du \langle \Gamma V, V \rangle \\ &= -\mathcal{F}v_1(L, t) - \int_0^L du \langle \Gamma V, V \rangle \leq -\mathcal{F}v_1(L, t), \end{aligned}$$

where we have used the compatibility condition, the covariant dynamics, the properties of the covariant derivative, and the positive definiteness of Γ . We see that in the absence of \mathcal{F} , this model is entirely dissipative, as expected. On the other hand, the $-\mathcal{F}v_1$ term at the boundary may, depending on its sign, inject energy into or dissipate energy from the rod.

V. LINEARIZED EQUATIONS

We first examine small-amplitude motions of the rod about the state of static equilibrium. We label quantities corresponding to this equilibrium with the suffix 0. Imposing the static condition $V_\alpha^{(0)} = (0, 0, 0)$ on the velocity and using the dynamical law and the boundary conditions yields

$$\Sigma_\alpha^{(0)} = (-\mathcal{F}, 0, 0), \quad E_\alpha^{(0)} = (\nu, 0, 0), \quad (17)$$

where $\nu = 1 - \mathcal{F}/k_1$ is a compression due to the applied pressure. The configuration corresponding to this state of deformation is obtained by integration

$$x^{(0)} = \nu u, \quad y^{(0)} = 0, \quad \theta^{(0)} = 0, \quad (18)$$

confirming that the rod remains undeflected and unsheared due to the applied pressure. We now proceed

with the linearization using the geometric procedure outlined in [31]. The result is

$$\begin{aligned} \Gamma_{\alpha\beta} \partial_t \xi_\beta &= \mathcal{D}_{\alpha\beta}^* [K_{\beta\mu} \mathcal{D}_{\mu\rho} \xi_\rho] + (\text{ad}_{\mathcal{D}\xi}^*)_{\alpha\beta} \Sigma_\beta^{(0)} \\ &\equiv \mathcal{M}_{\alpha\beta} \xi_\beta, \end{aligned} \quad (19)$$

where \mathcal{M} is the operator

$$\mathcal{M}_{\alpha\beta} = \begin{bmatrix} k_1 \partial_u^2 & 0 & 0 \\ 0 & k_2 \partial_u^2 & -(k_2 \nu + \mathcal{F}) \partial_u \\ 0 & (k_2 \nu + \mathcal{F}) \partial_u & k_3 \partial_u^2 - \nu(k_2 \nu + \mathcal{F}) \end{bmatrix} \quad (20)$$

and, as outlined in [31], the covariant derivatives are taken with respect to $E^{(0)}$. Note that the first order correction to the deformations $\mathcal{D}_{\alpha\beta} \xi_\beta = E_\alpha^{(1)}$ has components

$$h_1^{(1)} = \partial_u x^{(1)}, \quad h_2^{(1)} = \partial_u y^{(1)} - \nu \theta^{(1)}, \quad \Pi^{(1)} = \partial_u \theta^{(1)}. \quad (21)$$

The linearized boundary conditions are then the mixed boundary conditions on ξ

$$\xi_\alpha(0, t) = (0, 0, 0), \quad \mathcal{D}_{\alpha\beta} \xi_\beta(L, t) = (0, 0, 0). \quad (22)$$

We close this section by noting that the excess energy of the rod to first order in perturbation expressed in terms of the configuration is

$$\begin{aligned} \mathcal{U}_{\text{lin}} &= \frac{1}{2} \int_0^L du \langle K \mathcal{D}\xi, \mathcal{D}\xi \rangle \\ &= \frac{1}{2} \int_0^L du k_1(h_1^{(1)})^2 + k_2(h_2^{(1)})^2 + k_3(\Pi^{(1)})^2. \end{aligned} \quad (23)$$

Thus we may express the linearized equations as

$$\Gamma_{\alpha\beta} \partial_t \xi_\beta = -\frac{\delta \mathcal{U}}{\delta \xi_\alpha} + f_\alpha, \quad (24)$$

where

$$f_\alpha = \mathcal{F} \left(0, -\Pi^{(1)}, h_2^{(1)} \right),$$

showing that the linearized dynamics is a gradient flow for zero pressure, with a Timoshenko energy as the Lyapunov functional. On the other hand, the dynamics is circulatory for non-zero pressure, with the Timoshenko energy no longer a Lyapunov functional. The circulatory terms couple the vertical deflection and the angle, with the pressure acting as a source proportional to the bend, $\mathcal{F}\Pi^{(1)}$, in the deflection equation and as a sink proportional to the shear, $\mathcal{F}h_2^{(1)}$, in the angular equation. The circulatory character of the dynamics anticipates the instabilities and limit cycle oscillations we will uncover through the analyses below. The quadratic dependence on the pressure anticipates the non-monotonic variation of stability as the pressure is varied between the limits $0 \leq \mathcal{F} < k_1$. We now turn to establishing these results.

VI. LINEAR STABILITY ANALYSIS

To analyze the stability of the pre-stressed configuration, we expand the perturbations in Eq. (19) as

$$\xi_\alpha(u, t) = \text{Re} \left(\sum_{n=1}^{\infty} (\Xi_\alpha)_n(u) \exp(\lambda_n t) \right), \quad (25)$$

where $(\Xi_\alpha)_n = (X_n, Y_n, \Theta_n)$. This leads to the coupled generalized eigenvalue problem

$$\mathcal{M}_{\alpha\beta} \Xi_\beta = \lambda \Gamma_{\alpha\beta} \Xi_\alpha, \quad (26)$$

with generalized eigenmodes Ξ_α associated with generalized eigenvalues λ_n . Equivalently, we have the eigenvalue problem

$$\mathcal{L}_{\alpha\beta} \Xi_\beta = \lambda \Xi_\alpha \quad (27)$$

for $\mathcal{L}_{\alpha\beta} = \Gamma_{\alpha\mu}^{-1} \mathcal{M}_{\mu\beta}$, the generator of the dynamics. Furthermore, the eigenmodes Ξ_α satisfy the boundary conditions in Eq. (22). As shown in Appendix B, for $\mathcal{F} = 0$, $\mathcal{L}_{\alpha\beta}$ is Hermitian with respect to the Γ -inner product

$$(\psi, \xi)_\Gamma = \int_0^L du \langle \Gamma\psi, \xi \rangle, \quad (28)$$

where $\psi_\alpha, \xi_\alpha : [0, L] \rightarrow \mathbb{C}^3$ are vectors in a Hilbert space \mathcal{H} . Thus, for all $\psi_\alpha, \xi_\alpha \in \mathcal{H}$, $(\psi, \mathcal{L}\xi)_\Gamma = (\mathcal{L}\psi, \xi)_\Gamma$, and $\mathcal{L}^\dagger = \mathcal{L}$. Moreover, it is also negative definite, so $(\xi, \mathcal{L}\xi)_\Gamma \leq 0$ for all $\xi_\alpha \in \mathcal{H}$. Hence, in the absence of a follower force, the eigenvalues λ of $\mathcal{L}_{\alpha\beta}$ are strictly negative, leading to stable dynamics. On the other hand, Hermiticity is lost for $\mathcal{F} \neq 0$ and $\mathcal{L}^\dagger \neq \mathcal{L}$. This non-Hermiticity of $\mathcal{L}_{\alpha\beta}$ allows us to anticipate oscillatory and potentially unstable dynamics in the linear regime.

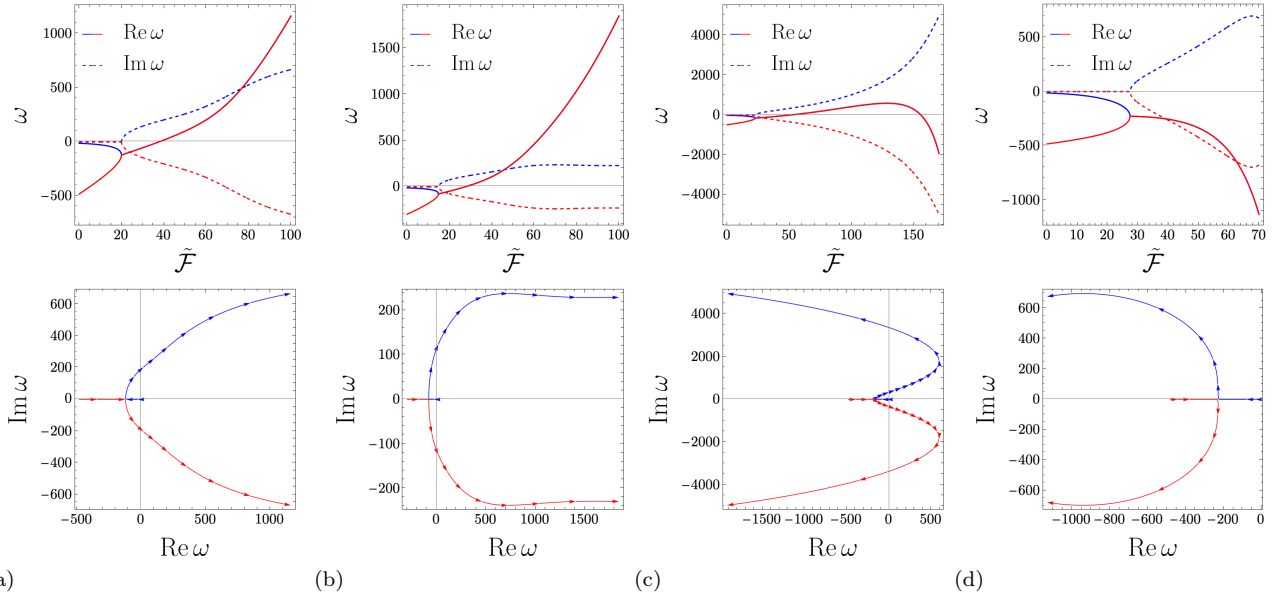


Figure 1: The first two roots, ω_1 (blue) and ω_2 (red), as a function of the strength of the follower force for the different combinations of parameters considered in Table I. The top plots show the real parts (solid lines) and the imaginary parts (dotted lines) of ω_1 and ω_2 . The corresponding plots at the bottom display the locus of ω_1 and ω_2 as the follower force parameter is swept. In (a), We find an onset of stable oscillations at $\tilde{\mathcal{F}} = 20.01$, after which ω_1 and ω_2 become complex conjugate pairs and $\omega_2 = \omega_1^*$. Stability is lost through a Hopf bifurcation, which is observed for $\tilde{\mathcal{F}}_{**} = 37.66$ when the real parts of the roots become positive and the roots cross the imaginary axis. A qualitatively similar behavior is observed in (b), where $\tilde{\mathcal{F}}_* = 14.80$ and $\tilde{\mathcal{F}}_{**} = 27.43$. In (c), we observe a qualitatively different behavior, where stability is lost through a Hopf bifurcation at $\tilde{\mathcal{F}}_{**} = 49.76$ but subsequently regained for $\tilde{\mathcal{F}} > 150$ when the real parts of the roots become negative again and the roots re-enter through the imaginary axis. Finally, in (d), although we find an onset of stable oscillations at $\tilde{\mathcal{F}}_* = 27.41$, stability is not lost through a Hopf bifurcation and no flutter instabilities are observed.

It is evident from the block structure of $\mathcal{L}_{\alpha\beta}$ that the

system decouples into a trivially stable diffusive longitu-

dinal component X_n and a non-trivial transverse component coupling Y_n and Θ_n . In other words, the system admits longitudinal eigenmodes $(X_n, 0, 0)$ with eigenvalues $\lambda_n^\parallel < 0$, and transverse eigenmodes $(0, Y_n, \Theta_n)$ with potentially complex eigenvalues λ_n^\perp . In what follows, we will adopt the notation $\omega_n \equiv \lambda_n^\perp$. The characteristic polynomial for the transverse subsystem, when lengths are non-dimensionalized by L , yields the dispersion relation

$$\begin{aligned} & \frac{\gamma_3}{k_2} \frac{\gamma_2 L^4}{k_3} \omega^2 \\ & - \left(\left(\frac{\gamma_2 L^2}{k_2} + \frac{\gamma_3 L^2}{k_3} \right) q^2 - \frac{\gamma_2 L^4}{k_3} \nu \left(\nu + \frac{\mathcal{F}}{k_2} \right) \right) \omega \quad (29) \\ & + q^4 + \frac{\mathcal{F} L^2}{k_3} \left(\nu + \frac{\mathcal{F}}{k_2} \right) q^2 = 0, \end{aligned}$$

from which we identify the shortest time scale τ_1 and the longest time scale τ_2 associated with the problem

$$\tau_1 = \frac{\gamma_3}{k_2}, \quad \tau_2 = \frac{\gamma_2 L^4}{k_3}. \quad (30)$$

Any choice of non-dimensionalization yields dimensionless stiffness and friction tensors $\tilde{K}_{\alpha\beta}, \tilde{\Gamma}_{\alpha\beta}$. For convenience, we adopt the time scale τ_1 for the nonlinear simulations, and reserve τ_2 for the linear stability analysis we will describe below. We denote non-dimensionalized constitutive parameters as in the components of $\tilde{K}, \tilde{\Gamma}$ by tildes, but we omit this notation for the degrees of freedom (x, y, θ) for clarity of notation. Adopting the time scale τ_2 leads to the non-dimensionalized parameters

$$\tilde{k}_1 = \frac{k_1 L^2}{k_3}, \quad \tilde{k}_2 = \frac{k_2 L^2}{k_3}, \quad \tilde{k}_3 = 1 \quad (31)$$

for the stiffness,

$$\tilde{\gamma}_1 = \frac{\gamma_1}{\gamma_2}, \quad \tilde{\gamma}_2 = 1, \quad \tilde{\gamma}_3 = \frac{\gamma_3}{\gamma_2 L^2} \quad (32)$$

for the friction, and

$$\tilde{\mathcal{F}} = \frac{\mathcal{F} L^2}{k_3} \quad (33)$$

for the follower force. Let $P = (\tilde{k}_1, \tilde{k}_2, \tilde{\gamma}_3)$ denote the tuple of constitutive parameters associated with the transverse subsystem. An application of the boundary conditions on (Y, Θ) as in Appendix C allows us to locate the eigenvalues ω_n of the system through the transcendental equation

$$B_1 + B_2 \sinh \chi_1 \sin \chi_2 + B_3 \cosh \chi_1 \cos \chi_2 = 0, \quad (34)$$

where $B_1, B_2, B_3, \chi_1, \chi_2$ are functions of ω , P , and $\tilde{\mathcal{F}}$, and are obtained explicitly in Appendix C.

To investigate the spectrum of \mathcal{L} , we fix a particular physical regime of the Cosserat rod by specifying a tuple of constitutive parameters P , and carrying out a sweep of

Figure	\tilde{k}_1	\tilde{k}_2	$\tilde{\gamma}_3$	Description
1	10^4	10^4	10^{-4}	Inextensible, Unshearable
2	10^4	10^2	10^{-2}	Shearable
3	2×10^2	10^4	10^{-4}	Extensible
4	10^2	10^4	10^{-4}	Extensible

Table I:
The range of constitutive parameters $(\tilde{k}_1, \tilde{k}_2, \tilde{\gamma}_3)$ corresponding to Fig. 2. Control over the elastic moduli allows us to investigate the effects of planar Cosserat degrees of freedom (stretch and shear).

$\tilde{\mathcal{F}}$ to control the strength of the follower force while locating the roots of the transcendental equation. We show the variation of the two smallest roots (in magnitude) ω_1, ω_2 of the transcendental equation. In particular, we consider the physical parameters P in Table I.

The range parameters P is chosen to investigate the effect of the Cosserat degrees of freedom on the spectrum, and the parameters $(\tilde{k}_1, \tilde{k}_2, \tilde{\gamma}_3) = (10^4, 10^4, 10^{-4})$ precisely recover the Euler-Bernoulli beam limit of a Cosserat rod, where the frame of directors is locked to the Frenet-Serret frame of the underlying centerline. This limit is discussed in detail in Section VIII.

We first investigate the spectrum for $\tilde{k}_1 = 10^4$. As shown in Fig. 1a, for $\tilde{k}_2 = 10^4, \tilde{\gamma}_3 = 10^{-4}$, we recover the classic flutter instability Hopf bifurcation diagram observed in the overdamped dynamics of planar inextensible filaments as in [17]. Namely, we find an onset of stable oscillations at a critical value of the follower force $\tilde{\mathcal{F}} = 20.01$, followed by a Hopf bifurcation/flutter instability at a second critical value $\tilde{\mathcal{F}} = 37.66$. On the other hand, as shown in Fig. 1b, allowing shear and angular dissipation through setting $\tilde{k}_2 = 10^2, \tilde{\gamma}_3 = 10^{-2}$ also recovers a qualitatively similar but quantitatively different bifurcation pattern. In particular, we now find that the onset of oscillations occurs for $\tilde{\mathcal{F}} = 14.80$ and $\tilde{\mathcal{F}} = 27.43$. For completeness, we also compute and illustrate the transverse eigenmodes and their associated deformations for different values of $\tilde{\mathcal{F}}$ in Fig. 5 – 7 in Appendix C. To understand the impact of shear and angular dissipation on the critical values of the follower force, we carry out a sweep of \tilde{k}_2 and $\tilde{\gamma}_3$. As shown in Fig. 2, We find that both critical values of \mathcal{F} increase monotonically as a function of \tilde{k}_2 and $1/\tilde{\gamma}_3$, plateauing at their Euler-Bernoulli values for sufficiently large \tilde{k}_2 and sufficiently small $\tilde{\gamma}_3$.

Next, we investigate the spectrum for Cosserat rods that can sustain greater compression, which corresponds to taking smaller values of \tilde{k}_1 . As illustrated in Fig. 1c, the parameters $(\tilde{k}_1, \tilde{k}_2, \tilde{\gamma}_3) = (2 \times 10^2, 10^4, 10^{-4})$ lead to a qualitatively different dependence of the spectrum on the follower force. Indeed, while we still observe an onset of damped oscillations (for $\tilde{\mathcal{F}} = 22.48$) followed by a Hopf bifurcation (for $\tilde{\mathcal{F}} = 49.76$), the window of flutter instability is now finite, terminating for

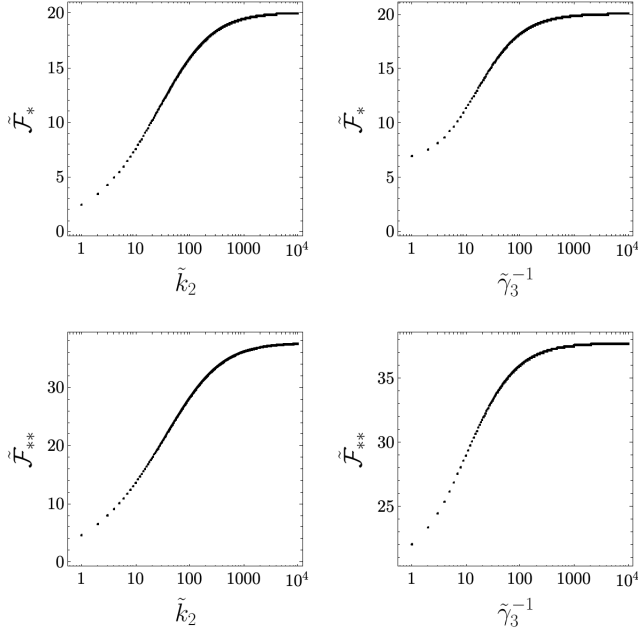


Figure 2: Semilog plots of the critical values of the follower force strength as a function of \tilde{k}_2 and $\tilde{\gamma}_3^{-1}$.

$\tilde{\mathcal{F}} > 150$. In this regime, which corresponds to a highly compressed Cosserat rod, we find that the follower force has a destabilizing effect followed by a stabilizing effect. On the other hand, as illustrated in Fig. 1d, the parameters $(\tilde{k}_1, \tilde{k}_2, \tilde{\gamma}_3) = (10^2, 10^4, 10^{-4})$ show only an onset of damped oscillations, and an absence of the Hopf bifurcation. The bifurcation structure is most sensitive to the variation of \tilde{k}_1 and the limit cycle oscillations can be entirely eliminated by an appropriate choice of this parameter. While this is a mathematically sound result based on a mathematically valid constitutive law, we should note that we have assumed a linear constitutive law for all values of the compression ratio $\nu = 1 - \tilde{\mathcal{F}}/\tilde{k}_1$. Large values of compression may lead to a breakdown of the linear constitutive law.

VII. NUMERICAL SIMULATIONS

Having established the appearance of a linear instability through a Hopf bifurcation in the previous section, we now carry out fully nonlinear simulations of the equations of motion to study the dynamics of Cosserat rods for large follower forces in the unstable regime. This allows us to determine the fate of the linear instability in

regions where the linear stability analysis is no longer valid. We employ the compatibility conditions for the simulations as outlined in Section III. In particular, we solve the nonlinear system of PDEs in Eq. (13) as a nonlinear hyperbolic time evolution system for (φ, E)

$$\partial_t \varphi = \varphi V(E), \quad \partial_t E_\alpha = \mathcal{D}_{\alpha\beta} V_\beta(E) \quad (35)$$

subject to the boundary conditions in Eq. (14), where the velocity is eliminated via Eq. (9). We non-dimensionalize the nonlinear system of PDEs by means of the short time scale τ_1 and the rest length L . We numerically solve the overdamped equations of motion using a Chebyshev spectral collocation on Mathematica, where we semi-discretize the partial differential equations in space to obtain a system of ordinary differential equations in time. These are solved at the interior nodes simultaneously with the algebraic equations that result from imposing the boundary conditions at the two boundary nodes. The numerical method is validated against the linear stability analysis and excellent agreement is obtained in the stable regime of the spectrum for the ranges of constitutive parameters considered in Section VI.

In the unstable regime of the spectrum, past the Hopf bifurcation, we find that the Cosserat rod carries out a self-sustaining beating motion of constant amplitude corresponding to a limit cycle. We excite the nonlinear oscillations in the rod by using the first eigenmodes obtained in the linear stability analysis to form appropriate initial conditions. For the initial-boundary value problem to be well-posed, one requires that the initial condition satisfies the nonlinear boundary conditions of the problem. We circumvent this by introducing a small dimensionless parameter $\epsilon \ll 1$ and imposing the initial data on (φ, E)

$$\varphi = \begin{bmatrix} 1 & 0 & 0 \\ \nu u & \cos(\epsilon \operatorname{Re} \Theta_1) & -\sin(\epsilon \operatorname{Re} \Theta_1) \\ \epsilon \operatorname{Re} Y_1 & \sin(\epsilon \operatorname{Re} \Theta_1) & \cos(\epsilon \operatorname{Re} \Theta_1) \end{bmatrix}, \quad E = \varphi^{-1} \partial_u \varphi. \quad (36)$$

The boundary conditions are then satisfied by the initial data to first order in the dimensionless parameter ϵ . The limit cycles are illustrated in Fig. 3 for $\tilde{\mathcal{F}}$ for a Cosserat rod with minimal compression that can sustain shear. We plot the amplitudes of the coordinates of the tip of the rod to illustrate the tip displacement, as well as snapshots of the entire Cosserat rod through the simulation. Additionally, for completeness, we carry out a sweep of the follower force $\tilde{\mathcal{F}}$ to obtain the displacement amplitude of the coordinates of the tip as a function of $\tilde{\mathcal{F}}$. The results are illustrated in Fig. 4.

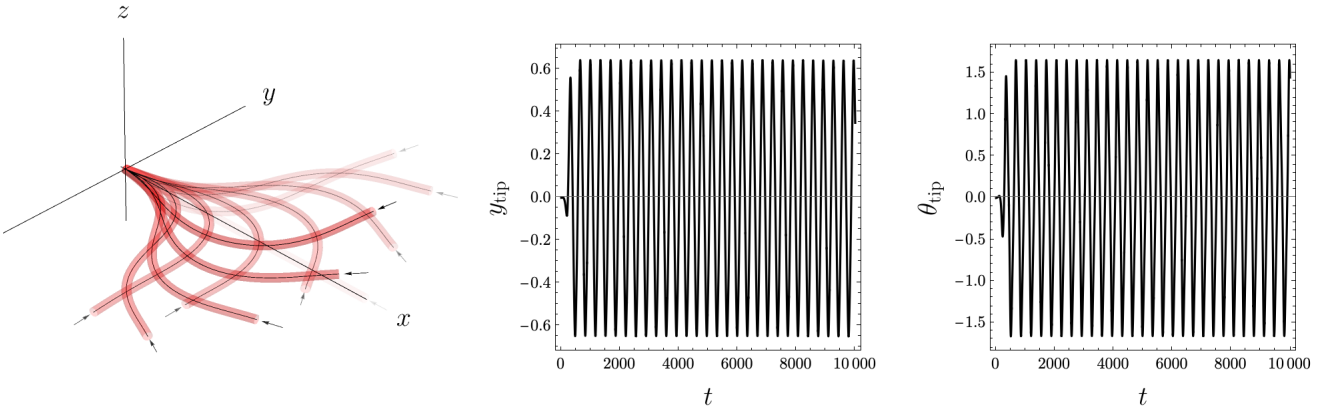


Figure 3: Emergence of limit cycle oscillations of the entire rod (left) and of the top of the rod (right) for $(\tilde{k}_1, \tilde{k}_2, \tilde{\gamma}_3) = (10^4, 10^2, 10^{-2})$ and $\tilde{\mathcal{F}} = 50$. Time is measured in units of τ_1 in the plots of the tip coordinates. For the visualization of the rod, the color scale is such that later snapshots of the rod are darker. The arrows indicate the configuration-dependent direction of the follower force at each time slice.

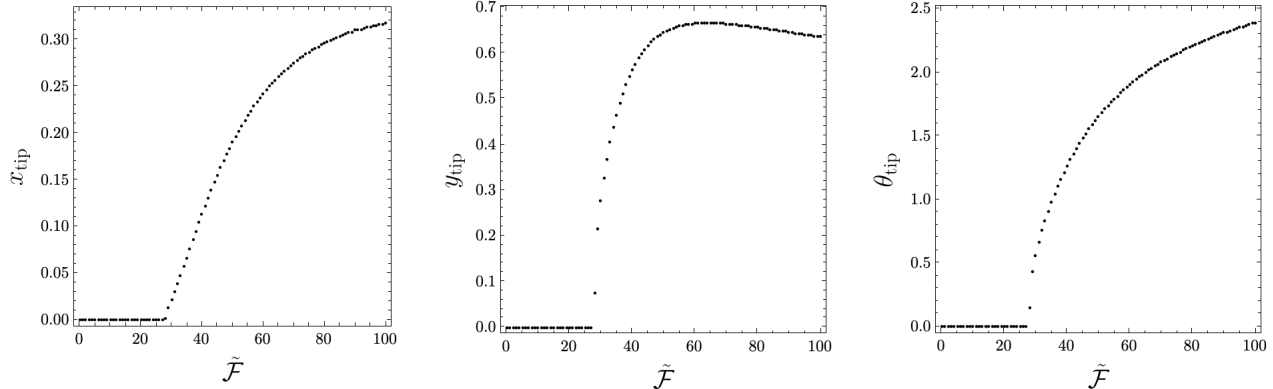


Figure 4: The steady-state limit cycle amplitudes of the coordinates of the tip of the rod as a function of the strength of the follower force.

VIII. EULER-BERNOULLI LIMIT

We derive the linearized equations of motion when the time scales are separated and show that it recovers the Euler-Bernoulli beam limit considered in the literature. We consider the limit of rapid relaxation of $\theta^{(1)}$ in which

$$0 = k_3 \partial_u^2 \theta^{(1)} + (k_2 \nu + \mathcal{F}) (\partial_u y^{(1)} - \nu \theta^{(1)}). \quad (37)$$

Differentiating once gives

$$0 = k_3 \partial_u^3 \theta^{(1)} + (k_2 \nu + \mathcal{F}) \partial_u (\partial_u y^{(1)} - \nu \theta^{(1)}). \quad (38)$$

Thus the equation for $y^{(1)}$ may be written as

$$\gamma_2 \partial_t y^{(1)} = -\frac{k_2 k_3}{(k_2 \nu + \mathcal{F})} \partial_u^3 \theta^{(1)} - \mathcal{F} \partial_u \theta^{(1)}. \quad (39)$$

We may then obtain the limit of vanishing shear through taking the limit $k_2 \rightarrow \infty$ and noting that in this limit,

$$\partial_u y^{(1)} = \nu \theta^{(1)}. \quad (40)$$

Thus we obtain the closed system of equations for the centerline

$$\begin{aligned} \gamma_1 \partial_t x^{(1)} &= k_1 \partial_u^2 x^{(1)}, \\ \gamma_2 \partial_t y^{(1)} &= -\frac{k_3}{\nu^2} \partial_u^4 y^{(1)} - \frac{\mathcal{F}}{\nu} \partial_u^2 y^{(1)}, \end{aligned} \quad (41)$$

and we note that the ν scaling increases the effective bending stiffness of the rod for large values of the follower force. This intuitively explains why the spectrum of the rod is stabilized when the stretch degree of freedom is allowed in the system. On the other hand, in the limit of vanishing stretch $k_1 \rightarrow \infty$, we find that $\nu = 1$ and

$$\gamma_2 \partial_t y^{(1)} = -k_3 \partial_u^4 y^{(1)} - \mathcal{F} \partial_u^2 y^{(1)}, \quad (42)$$

which is in agreement with the set up for this problem for filaments in the literature [17, 21, 23]. In both of these limits, the elimination of $\theta^{(1)}$ from the boundary conditions in Eq. (22) leads to the boundary conditions

$$\begin{aligned} y^{(1)}|_{u=0} &= \partial_u y^{(1)}|_{u=0} = 0, \\ \partial_u^2 y^{(1)}|_{u=L} &= \partial_u^3 y^{(1)}|_{u=L} = 0. \end{aligned} \quad (43)$$

IX. DISCUSSION AND CONCLUSION

Motivated by recent studies on follower forces in filaments on the one hand and the geometric field theory literature on the other hand, we have formulated a geometrically exact model of pressure-driven soft robotic arms in viscous fluids at low Reynold number. We formulate our model of a soft robotic arm as a Lie group-valued dissipative field theory, which leads to compact, coordinate-invariant expressions for the equations of motion from which convenient coordinatizations may be derived. In this process, we generalize the classic follower force model for filaments studied in the biophysics and soft matter physics literature to Cosserat rods that can sustain shear and stretch.

We have found that the linearization of this dissipative field theory leads to non-Hermitian physics in the presence of follower forces and to oscillatory dynamics. Our choice of constitutive law for the robotic arm allows us to exploit planar Cosserat degrees of freedom in their full generality and thus allows us to investigate the impact of shear, stretch, and bend on the spectrum of the linearized theory. Our investigations show excellent agreement with the established literature when these additional degrees of freedom are eliminated - namely, an onset of oscillatory relaxation followed by a Hopf bifurcation to stable limit cycle oscillations. On the other hand, departure from the filament regime leads to spectra that can be substantially different. We have found that incorporating stretch and shear shifts the critical values of the follower force monotonically downwards. More crucially, we have found that the stretch degree of freedom significantly alters the dynamical state diagram of the model. In the presence of stretch, the limit cycle is stable only when the magnitude of the follower force is in a finite interval bounded by a lower and an upper critical value. Outside this window, no stable oscillations exist and the rod relaxes to the linear configuration through damped oscillations. We have also identified a regime in parameter space where the Hopf bifurcation is absent and only decaying oscillations are obtained. These results illustrate the subtle nature of incorporating Cosserat degrees of freedom into the elastohydrodynamics of soft robotic arms. A beam limit that allows for stretch rationalizes seemingly counterintuitive phenomenon.

We carry out geometrically exact, nonlinear simulations of the robotic arm by leveraging the geometric field theory formalism that we used to model the problem. We formulate the governing nonlinear PDEs as a pair of time

evolution systems of PDEs that together constitute a nonlinear parabolic-hyperbolic system of equations. We leverage the Lie algebraic structure of velocities, deformations, and the covariant representation of the constitutive law to write down a time evolution equation for the deformation gradient E entirely in the Lie algebra. This is decoupled from another time evolution equation for our Cosserat field φ in the Lie group, which allows us to construct and visualize configurations of the robotic arm for all time. Our geometrically exact numerical integration scheme illustrates that in the linearly unstable regime of the spectrum, one obtains limit cycle oscillations of the robotic arm where the arm exhibits constant amplitude self-sustaining oscillations. There is excellent agreement between the analytical theory and the numerical results.

We highlight some future extensions of our present work. In a future publication, we shall carry out a perturbative expansion of the dissipative field theory to study the nature of the emergence of the limit cycle near the Hopf bifurcation. This allows us to analytically predict the amplitude of the limit cycle near the Hopf bifurcation. On the other hand, we shall also extend our geometric field theory formalism to three spatial dimensions for soft robotic arms that can also sustain torsion and twist. One may also investigate the effect of follower torques in three-dimensional models of soft robotic arms. Finally, one may generalize this dissipative field theory to arbitrary Lie groups G to study the dissipative mechanics of complex systems with Lie group-valued degrees of freedom. This would complement the conservative mechanics of such systems which have been studied extensively in the literature as G -snakes [32] and G -strands [33].

ACKNOWLEDGMENTS

We thank Professors M. E. Cates, R. E. Goldstein, and D. D. Holm for insightful discussions concerning mechanics and geometry. We thank Dr. Lukas Kikuchi, Balazs Nemeth, Mingjia Yan, and Hanchun Wang and for many helpful suggestions. We thank Professor M. C. Payne and Dr. A. Souslov for facilitating a collaboration between the Cavendish Laboratory and the Department of Applied Mathematics and Theoretical Physics. Mohamed Warda acknowledges a PhD studentship from the EPSRC/UKRI.

Appendix A: Geometric Conventions

We review the important properties associated with the geometric manipulations carried out in this paper. More details may be found in [31]. We use Greek indices throughout the paper for components of quantities that are in $\mathfrak{se}(2)$ or its dual, $\mathfrak{se}(2)^*$. We represent elements

$X \in \mathfrak{se}(2)$ as the 3×3 matrices

$$X = \begin{bmatrix} 0 & 0 & 0 \\ \zeta_1 & 0 & -\Lambda \\ \zeta_2 & \Lambda & 0 \end{bmatrix} = X_\alpha b_\alpha, \quad (\text{A1})$$

where $X_\alpha = (\zeta_1, \zeta_2, \Lambda)$ and b_α are the generators of the Lie algebra, which form a canonical basis of $\mathfrak{se}(2)$ and an associated dual basis b_α^* for $\mathfrak{se}(2)^*$. $\mathfrak{se}(2)$ is equipped with a Lie bracket $[\cdot, \cdot]$ which in our case is a matrix commutator $[X, Y] = XY - YX$. The structure constants $C_{\alpha\beta\mu}$ of $\mathfrak{se}(2)$ relative to its canonical basis are determined via the relations $[b_\alpha, b_\beta] = C_{\alpha\beta\mu} b_\mu$, which are given explicitly by

$$[b_1, b_2] = 0, \quad [b_3, b_1] = b_2, \quad [b_3, b_2] = -b_1. \quad (\text{A2})$$

The adjoint map is defined as

$$\text{ad}_X Y = [X, Y]. \quad (\text{A3})$$

We have a natural pairing between $\mathfrak{se}(2)^*$ and $\mathfrak{se}(2)$, $\langle \cdot, \cdot \rangle$, defined for $\sigma \in \mathfrak{se}(2)^*$, $X \in \mathfrak{se}(2)$ by

$$\langle \sigma, X \rangle = \sigma_\alpha X_\alpha, \quad (\text{A4})$$

through which we define the coadjoint ad^*

$$\langle \text{ad}_X^* \sigma, Y \rangle = -\langle \sigma, \text{ad}_X Y \rangle. \quad (\text{A5})$$

We note that for concrete calculations, the component-wise form of the pairing $\langle \cdot, \cdot \rangle$ is more useful. On the other hand, it is more convenient to preserve the component-free form of the pairing for more theoretical manipulations that are occasionally carried out in the paper.

We define the covariant derivatives

$$\begin{aligned} \mathcal{D} &= \partial_u + \text{ad}_E, \\ \mathcal{D}^* &= \partial_u + \text{ad}_E^*, \end{aligned} \quad (\text{A6})$$

which by construction satisfy the Leibniz rule

$$\partial_u \langle \sigma, X \rangle = \langle \mathcal{D}^* \sigma, X \rangle + \langle \sigma, \mathcal{D} X \rangle. \quad (\text{A7})$$

For concrete computations we make use of the canonical basis isomorphism in which we work relative to the basis b_α of $\mathfrak{se}(2)$, implicitly taking elements of both the Lie algebra and its dual to be column vectors in \mathbb{R}^3 (or \mathbb{C}^3 when studying the spectra of operators). For such computations, we find the matrix representations of the ad and ad^* operations to be

$$(\text{ad}_X)_{\alpha\beta} = \begin{bmatrix} 0 & -\Lambda & \zeta_2 \\ \Lambda & 0 & -\zeta_1 \\ 0 & 0 & 0 \end{bmatrix}, \quad (\text{ad}_X^*)_{\alpha\beta} = -(\text{ad}_X)_{\beta\alpha}, \quad (\text{A8})$$

and we work with the covariant derivatives as differential operator-valued matrices

$$\mathcal{D}_{\alpha\beta} = \delta_{\alpha\beta} \partial_u + (\text{ad}_E)_{\alpha\beta}, \quad \mathcal{D}_{\alpha\beta}^* = \delta_{\alpha\beta} \partial_u + (\text{ad}_E^*)_{\alpha\beta}. \quad (\text{A9})$$

For our particular set up of overdamped problems we are provided with the tensor $\Gamma : \mathfrak{se}(2) \rightarrow \mathfrak{se}(2)^*$ which we may interpret as a metric that allows us to induce an inner product on $\mathfrak{se}(2)$ itself via

$$X \cdot Y = \langle \Gamma X, Y \rangle = \Gamma_{\alpha\beta} X_\beta Y_\alpha. \quad (\text{A10})$$

This additionally allows us to define an inner product on the Hilbert space of functions valued in the Lie algebra, which is discussed in Appendix B.

Appendix B: Properties of \mathcal{L}

We work with the Γ -inner product defined on a Hilbert space of functions $\xi_\alpha : [0, L] \rightarrow \mathbb{C}^3$

$$(\psi, \xi)_\Gamma = \int_0^L du \langle \Gamma \psi, \xi \rangle, \quad (\text{B1})$$

where we extend the pairing in Eq. (A4) to allow for complex coefficients $\langle \Gamma \psi, \xi \rangle = \Gamma_{\alpha\beta} \psi_\beta^* \xi_\alpha$. It is straight forward to verify $\langle \Gamma \psi, \xi \rangle = \langle \Gamma \xi, \psi \rangle^*$ and $\langle K \psi, \xi \rangle = \langle K \xi, \psi \rangle^*$, which we implicitly use in the calculation below.

We obtain \mathcal{L}^\dagger through its definition $(\psi, \mathcal{L} \xi)_\Gamma = (\mathcal{L}^\dagger \psi, \xi)_\Gamma$ and its convenient expression in the form

$$\mathcal{L} \xi = \Gamma^{-1} (\mathcal{D}^* (K \mathcal{D} \xi) + \text{ad}_{\mathcal{D} \xi}^* \Sigma^{(0)}), \quad (\text{B2})$$

where

$$\mathcal{D} = \partial_u + \text{ad}_{E^{(0)}}. \quad (\text{B3})$$

We find through the properties of ad and \mathcal{D}

$$\begin{aligned} (\psi, \mathcal{L} \xi)_\Gamma &= \int_0^L du \left\langle \mathcal{D}^* (K \mathcal{D} \xi) + \text{ad}_{\mathcal{D} \xi}^* \Sigma^{(0)}, \psi \right\rangle^* \\ &= \langle K \mathcal{D} \xi, \psi \rangle^* \Big|_{u=0}^{u=L} - \left\langle K \mathcal{D} \psi + \text{ad}_\psi^* \Sigma^{(0)}, \xi \right\rangle \Big|_{u=0}^{u=L} \\ &\quad + \int_0^L du \left\langle \left(\mathcal{D}^* (K \mathcal{D} \psi) + \text{ad}_{\mathcal{D} \psi}^* \Sigma^{(0)} \right), \xi \right\rangle \\ &= \langle K \mathcal{D} \xi, \psi \rangle^* \Big|_{u=0}^{u=L} - \left\langle K \mathcal{D} \psi + \text{ad}_\psi^* \Sigma^{(0)}, \xi \right\rangle \Big|_{u=0}^{u=L} \\ &\quad + (\mathcal{L}^\dagger \psi, \xi)_\Gamma, \end{aligned} \quad (\text{B4})$$

where \mathcal{L}^\dagger is operationally identical to \mathcal{L}

$$\mathcal{L}^\dagger \psi = \Gamma^{-1} (\mathcal{D}^* (K \mathcal{D} \psi) + \text{ad}_{\mathcal{D} \psi}^* \Sigma^{(0)}). \quad (\text{B5})$$

Imposing that the boundary terms vanish and using the primal boundary conditions

$$\xi|_{u=0} = 0, \quad \mathcal{D} \xi|_{u=L} = 0 \quad (\text{B6})$$

produces the adjoint boundary conditions

$$\psi|_{u=0} = 0, \quad (K \mathcal{D} \psi + \text{ad}_\psi^* \Sigma^{(0)})|_{u=L} = 0, \quad (\text{B7})$$

which are different from the primal boundary conditions for $\mathcal{F} \neq 0$. Thus we see that for $\mathcal{F} \neq 0$, $\mathcal{L} \neq \mathcal{L}^\dagger$ since they act on different domains, and the system exhibits a loss of Hermiticity. On the other hand, for $\mathcal{F} = 0$, the domains of the two operators \mathcal{L} and \mathcal{L}^\dagger are identical, and we obtain $\mathcal{L} = \mathcal{L}^\dagger$ - in this case, \mathcal{L} is Hermitian and admits strictly real eigenvalues. Moreover, in the case that $\mathcal{F} = 0$, we immediately see that \mathcal{L} is necessarily a negative definite operator. Indeed, this is another manifestation of the conservation of energy

$$\begin{aligned} (\xi, \mathcal{L}\xi)_\Gamma &= \int_0^L du \langle \xi, \mathcal{D}^*(K\mathcal{D}\xi) \rangle \\ &= - \int_0^L du \langle K\mathcal{D}\xi, \mathcal{D}\xi \rangle \\ &\leq 0. \end{aligned} \quad (\text{B8})$$

Appendix C: Eigenvalues and Eigenvectors

We introduce the auxiliary quantity $\mu = \tilde{k}_2\nu + \tilde{\mathcal{F}}$ for convenience. The characteristic polynomial for the transverse subsystem corresponding to solutions of the form

$$\Xi_\alpha \sim \begin{bmatrix} 0 \\ A_1 \\ A_2 \end{bmatrix} \exp(\omega t) \exp(qu) \quad (\text{C1})$$

may be written, after non-dimensionalization, as the quartic equation in q

$$\frac{\tilde{k}_2}{\tilde{\gamma}_3} q^4 + \left(\tilde{\mathcal{F}}\mu - \left(\tilde{k}_2 + \frac{1}{\tilde{\gamma}_3} \right) \omega \right) q^2 + \omega(\omega + \nu\mu) = 0. \quad (\text{C2})$$

Thus we find that for a given value of ω , there are four associated roots $q \in \{\pm\chi_1, \pm i\chi_2\}$ of the quartic. Note that this convention is inspired by the case of $\tilde{\mathcal{F}} = 0$,

where $\omega < 0$ and $\chi_1, \chi_2 \in \mathbb{R}$. Thus, we may write

$$\begin{aligned} \Xi(u) &= C_1 \begin{bmatrix} 0 \\ \cosh \chi_1 u \\ g_1 \sinh \chi_1 u \end{bmatrix} + C_2 \begin{bmatrix} 0 \\ \sinh \chi_1 u \\ g_1 \cosh \chi_1 u \end{bmatrix} \\ &+ C_3 \begin{bmatrix} 0 \\ \cos \chi_2 u \\ -g_2 \sin \chi_2 u \end{bmatrix} + C_4 \begin{bmatrix} 0 \\ -\sin \chi_2 u \\ -g_2 \cos \chi_2 u \end{bmatrix}, \end{aligned} \quad (\text{C3})$$

where $C_1, C_2, C_3, C_4 \in \mathbb{C}$ are constants and g_1, g_2 are the auxiliary quantities

$$g_1 = \frac{\tilde{k}_2 \chi_1^2 - \omega}{\mu \chi_1}, \quad g_2 = \frac{\tilde{k}_2 \chi_2^2 + \omega}{\mu \chi_2}. \quad (\text{C4})$$

The boundary conditions

$$\begin{aligned} Y(0) &= \Theta(0) = 0, \\ Y'(1) - \nu \Theta(1) &= \Theta'(1) = 0, \end{aligned} \quad (\text{C5})$$

lead to a 4×4 system of linear equations for the constants C_i , which may be written as $\Delta_{ij} C_j = 0$ where Δ is a 4×4 matrix. The condition $\det \Delta = 0$ simplifies to the following transcendental equation for ω

$$B_1 + B_2 \sinh \chi_1 \sin \chi_2 + B_3 \cosh \chi_1 \cos \chi_2 = 0, \quad (\text{C6})$$

where

$$\begin{aligned} B_1 &= (\chi_1(\chi_1 - \nu g_1) - \chi_2(\chi_2 - \nu g_2))g_1, \\ B_2 &= -(\chi_2(\chi_1 - \nu g_1) + \chi_1(\chi_2 - \nu g_2))g_1, \\ B_3 &= \frac{\chi_2 g_2^2 (\chi_1 - \nu g_1) - \chi_1 g_1^2 (\chi_2 - \nu g_2)}{g_2}. \end{aligned} \quad (\text{C7})$$

The transcendental equation admits countably many solutions ω in the complex numbers for a given choice of constitutive parameters and follower force. For each such ω , we compute its associated eigenmode $\Xi = (0, Y, \Theta)$

$$\begin{aligned} Y(u) &= \mathcal{N} \left(\cosh \chi_1 u - \cos \chi_2 u - G \left(\frac{1}{g_1} \sinh \chi_1 u - \frac{1}{g_2} \sin \chi_2 u \right) \right), \\ \Theta(u) &= \mathcal{N} (g_1 \sinh \chi_1 u + g_2 \sin \chi_2 u - G (\cosh \chi_1 u - \cos \chi_2 u)), \end{aligned} \quad (\text{C8})$$

where

$$G = \frac{\chi_1 g_1 \cosh \chi_1 + \chi_2 g_2 \cos \chi_2}{\chi_1 \sinh \chi_1 + \chi_2 \sin \chi_2} \quad (\text{C9})$$

and \mathcal{N} is a choice of normalization. We choose \mathcal{N} such that $Y(1) = 1$.

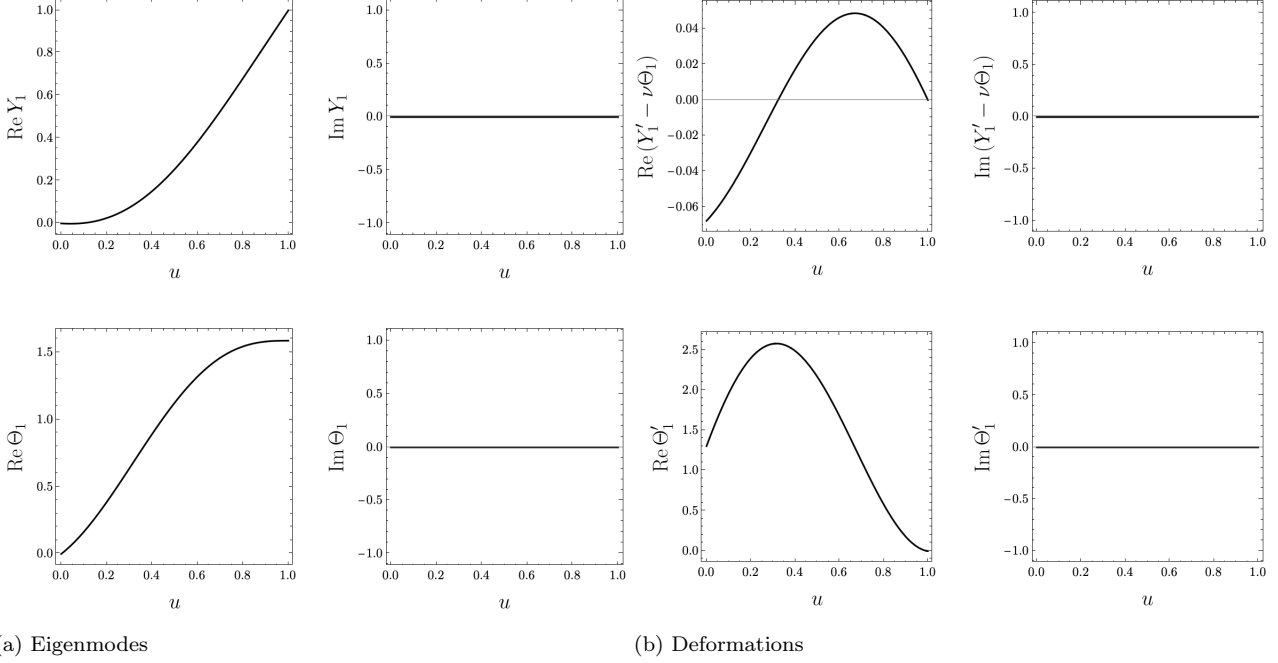


Figure 5: The first eigenmode $(0, Y_1, \Theta_1)$ and its associated deformations for $(\tilde{k}_1, \tilde{k}_2, \tilde{\gamma}_3) = (10^4, 10^2, 10^{-2})$ and $\tilde{\mathcal{F}} = 10$, before the onset of oscillations.

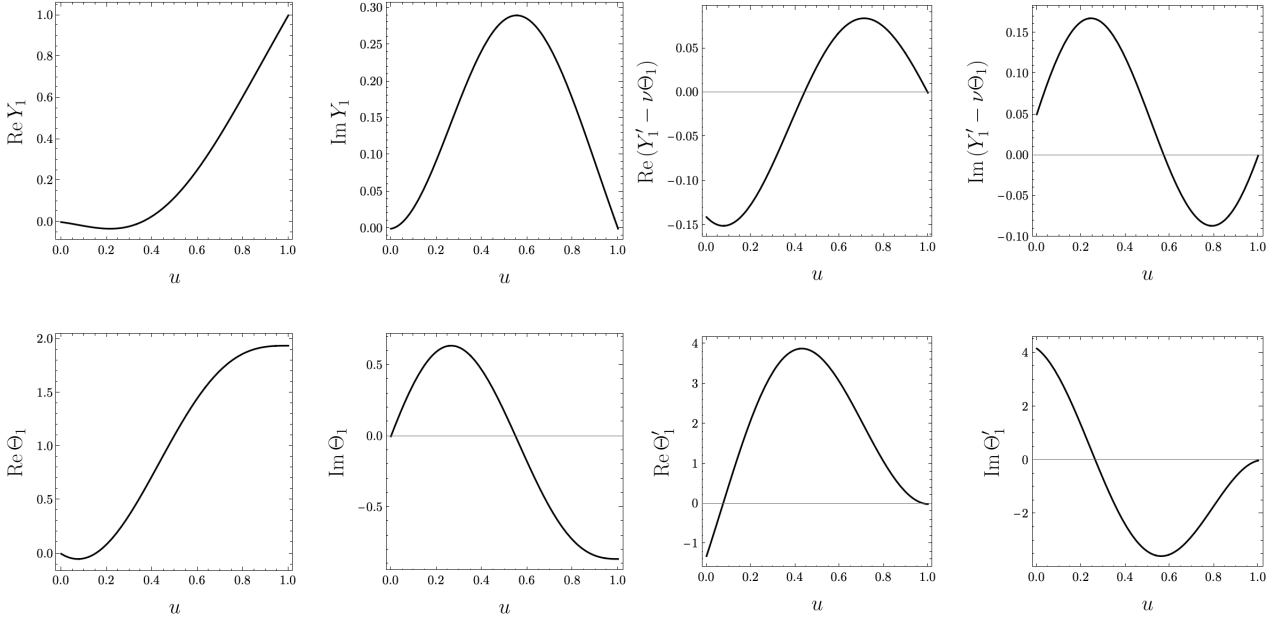


Figure 6: The first eigenmode $(0, Y_1, \Theta_1)$ and its associated deformations for $(\tilde{k}_1, \tilde{k}_2, \tilde{\gamma}_3) = (10^4, 10^2, 10^{-2})$ and $\tilde{\mathcal{F}} = 20$, after the onset of oscillations but before the Hopf bifurcation.

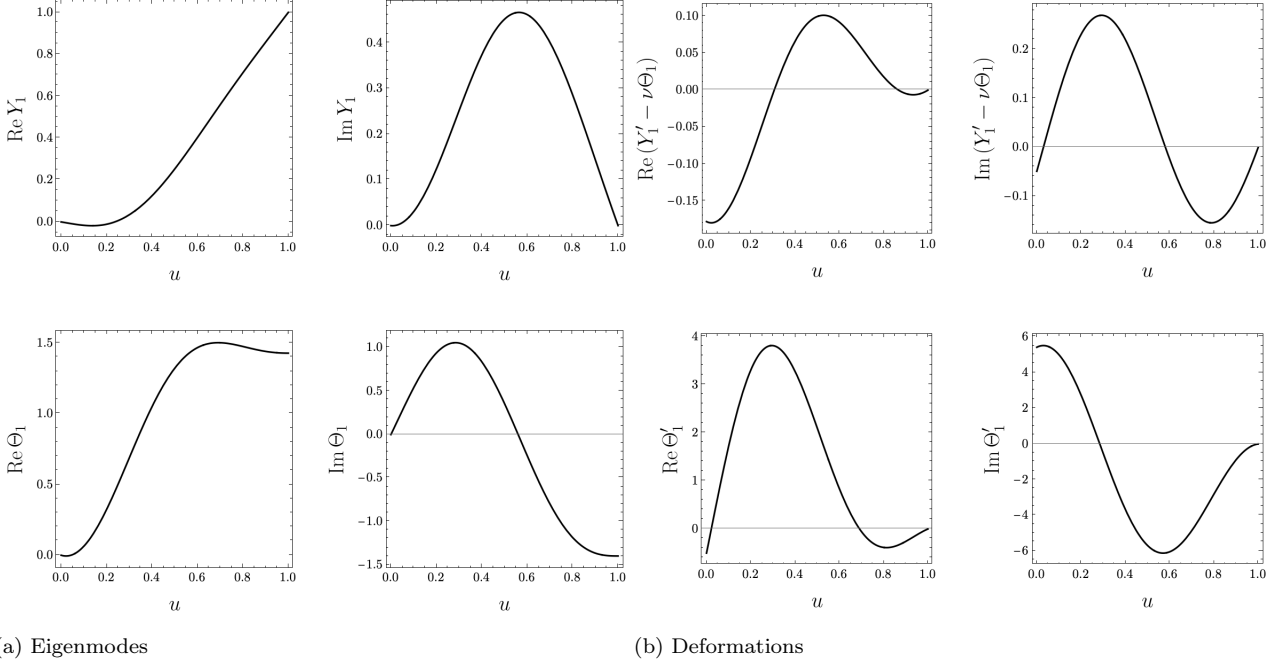


Figure 7: The first eigenmode $(0, Y_1, \Theta_1)$ and its associated deformations for $(\tilde{k}_1, \tilde{k}_2, \tilde{\gamma}_3) = (10^4, 10^2, 10^{-2})$ and $\tilde{\mathcal{F}} = 30$, after the Hopf bifurcation.

[1] R. M. Murray, *A Mathematical Introduction to Robotic Manipulation* (CRC Press, Boca Raton, 1994).

[2] J. M. Selig, *Geometric Fundamentals of Robotics* (Springer, New York, 2004).

[3] G. S. Chirikjian, *Stochastic Models, Information Theory, and Lie Groups, Volume 1: Classical Results and Geometric Methods* (Birkhäuser Boston, 2009).

[4] G. S. Chirikjian and J. W. Burdick, IEEE Robot. Autom. Mag. **1**, 22 (1994).

[5] T. Ranzani, M. Cianchetti, G. Gerboni, I. D. Falco, and A. Menciassi, IEEE Trans. Robot. **32**, 187 (2016).

[6] F. Campisano, A. A. Remirez, S. Caló, J. H. Chandler, K. L. Obstein, R. J. Webster, and P. Valdastri, IEEE Robot. Autom. Lett. **5**, 2642 (2020).

[7] F. Campisano, S. Caló, A. A. Remirez, J. H. Chandler, K. L. Obstein, R. J. WebsterIII, and P. Valdastri, Int. J. Robot. Res. **40**, 923 (2021).

[8] A. E. H. Love, *A Treatise on the Mathematical Theory of Elasticity* (Cambridge University Press, Cambridge, 1892).

[9] J. L. Erickson and C. Truesdell, Arch. Ration. Mech. Anal. **1**, 295 (1957).

[10] S. S. Antman, *Nonlinear Problems of Elasticity* (Springer, New York, 2005).

[11] M. Gazzola, L. H. Dudte, A. G. McCormick, and L. Mahadevan, R. Soc. Open Sci. **5**, 171628 (2018).

[12] F. Boyer, V. Lebastard, F. Candelier, and F. Renda, IEEE Trans. Robot. **37**, 847 (2021).

[13] N. Naughton, J. Sun, A. Tekinalp, T. Parthasarathy, G. Chowdhary, and M. Gazzola, IEEE Robot. Autom. Lett. **6**, 3389 (2021).

[14] Z. Chen, Z. Liu, and X. Han, Micromachines **13**, 1486 (2022).

[15] A. Tekinalp, Y. Bhosale, S. Cui, F. K. Chan, and M. Gazzola, Comput. Methods Appl. Mech. Eng. **440**, 117910 (2025).

[16] A. Laskar and R. Adhikari, New J. Phys. **19**, 033021 (2017).

[17] G. De Canio, E. Lauga, and R. E. Goldstein, J. R. Soc. Interface **14**, 20170491 (2017).

[18] F. Ling, H. Guo, and E. Kanso, J. R. Soc. Interface **15**, 20180594 (2018).

[19] Y. Man and E. Kanso, Soft Matter **15**, 5163 (2019).

[20] Y. Fily, P. Subramanian, T. M. Schneider, R. Chelakkot, and A. Gopinath, J. R. Soc. Interface **17**, 20190794 (2020).

[21] B. Clarke, Y. Hwang, and E. E. Keaveny, Phys. Rev. Fluids **9**, 073101 (2024).

[22] K. G. Link, R. D. Guy, B. Thomases, and P. E. Arratia, J. R. Soc. Interface **21**, 20240046 (2024).

[23] O. Schnitzer, J. Fluid Mech. **1007**, A65 (2025).

[24] M. Beck, Z. Angew. Math. Phys. **3**, 225 (1952).

[25] V. V. Bolotin, *Nonconservative Problems of the Theory of Elastic Stability*, edited by G. Herrmann (Pergamon Press, London, 1963).

[26] H. Ziegler, *Principles of Structural Stability* (Blaisdell Publishing Company, Waltham, MA, 1968).

[27] J. Carr and M. Z. M. Malhardeen, SIAM J. Appl. Math.

37, 261 (1979).

[28] M. Chen, Nonlinear Analysis: Theory, Methods & Applications **11**, 1061 (1987).

[29] H. Koch and S. S. Antman, SIAM J. Math. Anal. **32**, 360 (2000).

[30] Q. Wang, Int. J. Solids Struct. **41**, 4875 (2004).

[31] M. Yan, M. Warda, B. Németh, L. Kikuchi, and R. Adhikari, Geometric Field Theory for Elastohydrodynamics of Cosserat Rods (2025), (unpublished).

[32] P. S. Krishnaprasad and D. P. Tsakiris, in *Proceedings of the 33rd IEEE Conference on Decision and Control* (IEEE, Lake Buena Vista, FL, 1994) pp. 2955–2960.

[33] D. Holm, R. Ivanov, and J. R. Percival, J. Nonlinear Sci. **22**, 517 (2012).